Uptake of a fluorescent L-glucose derivative 2-NBDLG into three-dimensionally accumulating insulinoma cells in a phloretin-sensitive manner
(三次元的に集積したインスリノーマ細胞への蛍光 L-グルコース誘導体 2-NBDLG のフロレチン感受性取り込み)

申 請 者　弘前大学大学院医学研究科
脳神経科学領域　神経・脳代謝制御学教育研究分野
氏　　名　佐々木　綾子
指 導 教 授　蔵田　潔

ABSTRACT

Of two stereoisomers of glucose, only D- and not L-glucose is abundantly found in nature, being utilized as an essential fuel by most organisms. The uptake of D-glucose into mammalian cells occurs through glucose transporters such as GLUTs, and this process has been effectively monitored by a fluorescent D-glucose derivative 2-[*N*-(7-Nitrobenz-2-oxa-1,3-diazol-4-yl)amino]-2-deoxy-D-glucose (2-NBDG) at the single cell level. However, since fluorescence is an arbitrary measure, we have developed a fluorescent analogue of L-glucose 2-[*N*-(7-Nitrobenz-2-oxa-1,3-diazol-4-yl)amino]-2-deoxy-L-glucose (2-NBDLG), as a negative control substrate for more accurately identifying the stereoselectivity of the uptake.

Interestingly, a small portion of mouse insulinoma cells MIN6 abundantly took up 2-NBDLG at a late culture stage (> ~10 days *in vitro*, DIV) when multi-cellular spheroids exhibiting heterogeneous nuclei were formed, whereas no such uptake was detected at an early culture stage (< ~6 DIV). The 2-NBDLG uptake was persistently observed in the presence of a GLUT inhibitor cytochalasin B. Neither D- nor L-glucose in 50 mM abolished the uptake. No significant inhibition was detected by inactivating sodium/glucose cotransporters (SGLTs) with Na^+-free condition.

To our surprise, the 2-NBDLG uptake was totally inhibited by phloretin, a broad spectrum inhibitor against transporters/channels including GLUTs and aquaporins. From these, a question might be raised if non-GLUT/non-SGLT pathways participate in the 2-NBDLG uptake into spheroid-forming MIN6 insulinoma. It might also be worthwhile investigating whether 2-NBDLG can

be used as a functional probe for detecting cancer, since the nuclear heterogeneity is among critical features of malignancy.

INTRODUCTION

Mammalian cells take up D-glucose in a stereoselective manner through plasma membrane transporters such as GLUTs, whereby only D- and not L-glucose is recognized [1)]. We have shown that 2-[*N*-(7-Nitrobenz-2-oxa-1,3-diazol-4-yl)amino]-2-deoxy-D-glucose (2-NBDG) (Online Resource 1a), which was originally synthesized to see the viability of *E. coli* cells [2)], is taken up into mammalian cells through GLUTs in a time, concentration and temperature-dependent manner [3, 4)]. So far, 2-NBDG has been effectively utilized for monitoring D-glucose uptake in a variety of mammalian cells including pancreatic cells [3, 5)], brain cells [6-9)], and tumor cells [10-15)]. However, since fluorescence is an arbitrary measure, a control substrate has been awaited for more accurately evaluating the GLUT-mediated component [4)].

A green fluorescence-emitting 2-[*N*-(7-Nitrobenz-2-oxa-1,3-diazol-4-yl)amino]-2-deoxy-L-glucose (2-NBDLG), the mirror-image isomer of 2-NBDG, was thus developed as the control substrate (Online Resource 1b) [16, 17)]. For evaluating an occurrence of non-specific uptake such as due to a loss of membrane integrity, we found it strongly helpful to use 2-NBDLG simultaneously with a membrane-impermeable L-glucose derivative 2-TRLG, which bears a large red fluorophore Texas red (Online Resource 1c) [17)].

To explore the stereoselective uptake of mammalian cells with such fluorescent tracers, we have used mouse insulin-secreting clonal (MIN6) cells [18)]. Surprisingly, when MIN6 cells cultured over 10

days *in vitro* (DIV) were examined, the fluorescence of cells increased significantly not only by application of 2-NBDG, but also by 2-NBDLG. In the present study, we characterize unique features of the 2-NBDLG uptake into the insulinoma cells.

METHODS

Confocal microscopic study

Culture

MIN6 cells were grown, according to the original protocol in Dulbecco's modified Eagle's medium (DMEM) (D5648, Sigma-Aldrich) [18]. Only cells in earlier passages (from 5 up to 10 times) were used in the present study except for Online Resource 2 [19]. On the day of culture, poly-L-lysine hydrobromide (PLL) (P6282, final concentration 1/500, Sigma)-coated, small glass coverslips (No. 0, Matsunami) were placed on 35 mm non-coated dish (Iwaki). Cells for the confocal measurement were seeded at a density of 1000 cells per cover slip. Culture medium was half exchanged every 3 days.

Measurement

The tracer application and image acquisition were conducted by modifying the method reported previously [4, 17]. In brief, a temperature-controlled custom made chamber was placed on a motor-driven xyz stage of a laser confocal microscope (TCS-SP5, Leica). 2-NBDG/2-NBDLG and 2-TRLG were excited by a single 488 nm laser source and the fluorescence was detected in 500-580 nm and 580-740 nm wavelength range, respectively, with a dichroic mirror at 500 nm (RSP 500). 4',6-diamidino-2-phenylindole (DAPI) was applied for nuclear staining in live-cell condition at 37ºC.

An objective lens HCX PL APO 40x/1.25-0.75 OIL was used except for Online Resource 2 and 7, for which HC PL APO 20x/0.70 IMM was used.

Fluorescence microplate reader experiments

Culture

MIN6 cells were seeded at a density of 6000 cells/well on 96-well clear-bottom plate (μClear-plate #655090, Greiner Bio-One). Wells in columns 3 and 5 (rows from B to F, total 12 wells) were used for culture and no cell was seeded in the top (A) and the bottom (H) rows in these columns. Typically, 10 μl of cell suspension was plated at 6 x 10^5 cells/ml on the center of each well, left for 20 minutes in CO_2 incubator at 37ºC, 200 μl of DMEM was then added to each well. Cells incubated for 10-14 DIV were used for measurement.

Measurement

For the measurement of the tracer uptake, a fluorescence microplate reader was used with its operation software (FlexStation and SoftMax Pro, Molecular Devices). The fluorescence was measured three times from the bottom of the plate and was averaged. Excitation, emission, and cut off wavelength were 470nm, 540 nm, and 495 nm, respectively.

Just before measurements, culture medium was removed from each well leaving 50μl. Cells were then washed five times with 200 μl of standard Krebs Ringer Buffer Solution (KRB) (in mM; 129

NaCl, 4.8 KCl, 1.2 KH_2PO_4, 1.2 $MgSO_4$, 1.0 $CaCl_2$, 10 HEPES, 5.0 $NaHCO_3$, 5.6 D-glucose, 0.1 carbenoxolone, pH 7.30 - 7.35) at room temperature (26 ± 1ºC). After the fifth wash, KRB was added to adjust the height of solution to that of blank wells in column 4, in which in which 200µl of KRB without containing tracers was added. Nine regions of interest (ROIs, 1.5 mm in diameter, each contained typically ~5000 cells or more when measured at 12 DIV) were preset in single wells of 96-well plate. By visualizing cells before and after the experiment with a flatbed scanner (GT-X820, Seiko Epson), ROIs, in which cells were unevenly seeded or lost during washout, were excluded from the analysis.

Autofluorescence was measured for individual ROIs. According to a precisely timed protocol, 50 µl of 2-NBDG- or 2-NBDLG-containing KRB solution (400 µM) was then added into 8 wells from A to H in column 3, in which 50 µl of KRB was pre-loaded, by using a calibrated 8-channel pipette (final concentration, 200 µM). 30 seconds later, fluorescent tracers were similarly added to wells in column 5. The top (A) and bottom (H) wells in columns 3 and 5 were used as control to check that the tracer was successfully washed out from the solution. After adding the tracer solution, the plate was quickly placed on the tray in FlexStation at 37ºC. Five minutes later, 50 µl of the tracer solution was removed from wells in column 3, and 300 µl of KRB solution was added at room temperature. Thirty seconds later, similar washout process was done in column 5. After repeating this process 7 times, 300 µl of KRB was finally added and 150 µl of KRB was removed, the fluorescence was then measured and

compared among ROIs. Transient increase in fluorescence due to a loss of membrane integrity decreased to a large extent during this washout procedure.

For Na^+-free experiments, NaCl in KRB was replaced by choline chloride. For glucose competition assay, 50 mM of D- or L-glucose solution was prepared by reducing NaCl so that the osmolality of the solution was identical to that of control.

Reagents

2-NBDLG (23003-v, Peptide Institute), 2-NBDG (23002-v, Peptide Institute), and 2-TRLG were provided by Peptide Institute Inc. and used as described previously [17]. Carbenoxolone (C4790, Sigma) was used to block gap junction/hemi-channel. Phloretin (P7912, Sigma), cytochalasin B (C6762, Sigma), and 4,6-*O*-ethylidene-D-glucose (E0402, Tokyo Chemical Industry) were applied prior to the tracer application. DAPI (D523, Wako) was added in some experiments for nuclear staining. pSIVA-IANBD (IMGENEX) and propidium iodide (IMGENEX) were used as a polarity-sensitive, real time marker for apoptotic cells and an indicator for necrotic cells, respectively, according to manufacturer's instruction. NBD-NH_2 was synthesized by the reaction of NBD-F and ammonia. NBD-OH was obtained as a by-product on the synthesis of 2-NBDLG. Both NBD-NH_2 and NBD-OH were used at a final concentration of 200 μM.

Statistics

ANOVA and Bonferroni-Dunn test were used. Error bars represent SD.

RESULTS

Imaging of 2-NBDG and 2-NBDLG uptake with confocal microscopy

MIN6 cells, when seeded at a very low density (1000 cells per coverslip), formed small three-dimensional spheroid after several days (Fig. 1a,e). At 6 DIV, a brief superfusion with 100 μM of 2-NBDG solution for 3 minutes followed by washout increased the cellular fluorescence in varying intensity among cells (Fig. 1b-d). Such unique heterogeneity in the 2-NBDG uptake is very different from relatively homogeneous uptake of the tracer in two-dimensionally spreading MIN6 cells (Online Resource 2). By contrast, no such increase in the fluorescence was detected by similarly applying 100 μM of 2-NBDLG (L-form isomer) solution (Fig. 1e-h), although one may notice cells showing faint fluorescence if examined closely (asterisks in Fig. 1e-h).

Interestingly, more drastic 2-NBDLG uptake was detected at 10-15 DIV, when much thicker (> 50 μm-thick) spheroids were grown (A in Fig. 2). Of two similarly shaped MIN6 spheroids (A and B in Fig. 2a), only upper one showed remarkable 2-NBDLG uptake (Fig. 2b,d), whereas lower one increased fluorescence only slightly.

Nuclear staining with DAPI in live-cell condition further revealed that the upper spheroid consisted of heterogeneous cells, including large cells which bear unusually large and strongly DAPI-positive nucleus as well as small cells having nucleus of ordinary size (Fig. 2e,f, see also Online Resource 4).

By contrast, the lower spheroid consisted of cells bearing evenly sized small nuclei that were only weakly positive for DAPI (B in Fig. 2e,f).

It is noteworthy that 2-NBDLG was taken up not only into such large presumably multinucleated cells but also into small cells having nucleus of ordinary size (Fig. 2d,f). DAPI-positive, fibrous processes were seen in the upper spheroid, in addition (Online Resource 4) [20]. Similar fibrous processes appeared in other clusters that occasionally took up 2-NBDLG (asterisks in Fig. 2e and Online Resource 4).

Quantitative evaluation of the 2-NBDG and 2-NBDLG uptake by a fluorescent microplate reader

Thick and large spheroids easily collapsed sometimes in hours. Moreover, whether or not spheroids of interest would take up abundant 2-NBDLG was difficult to be expected prior to imaging. Thus, we evaluated the average fluorescence intensity of a large number of MIN6 cells subjected to 2-NBDLG comparing with those subjected to 2-NBDG at 10-14 DIV by using a fluorescent microplate reader.

When 200 μM of 2-NBDG was applied for 5 minutes, the average fluorescence intensity of ROIs increased from 1.6 ± 0.4 arbitrary unit (A.U., autofluorescence) to 12.2 ± 2.6 A.U. ($n = 48$, $p < 0.0001$, Fig. 3a). 2-NBDLG, applied simultaneously but to other wells, also noticeably increased the fluorescence from 1.7 ± 0.5 A.U. to 6.7 ± 1.6 A.U. ($n = 51$, $p < 0.0001$, Fig. 3a). Measurements were

performed in quadruplicate and the ratio of the net increase in the fluorescence for 2-NBDLG to that for 2-NBDG was 44.9 ± 1.7 % in average (Fig. 3b).

Cytochalasin B, which acts as a GLUT inhibitor when used at a low dose (10 μM), significantly decreased the 2-NBDG uptake into MIN6 cells ($p < 0.0001$, Fig. 3c). 2-NBDG uptake was decreased by 61.9 ± 3.9 % in average in the presence of cytochalasin B in experiments performed in triplicate. On the other hand, 2-NBDLG uptake on the same plates was attenuated only slightly by 20.5 ± 9.6 % in the presence of cytochalasin B (Fig. 3c). Interpreted another way, in the presence of cytochalasin B, the substantial component remained in the uptake of 2-NBDLG, and that of 2-NBDG as well, implicating an involvement of non-GLUT mechanisms for both uptake of the L- as well as D-derivatives.

Consistently, a large amount of D-glucose (50 mM) reduced the 2-NBDG uptake only moderately by 28.9 ± 12.4 % ($p < 0.0001$, Online Resource 3a), and no inhibition was detected by the same amount of L-glucose. Similarly to in Fig. 3c, 2-NBDLG uptake was attenuated only slightly by 50 mM D-glucose (Online Resource 3b). The same amount of L-glucose showed no effect on the uptake. An involvement of SGLTs, energy-demanding Na^+-coupled glucose transporters, is unlikely, since both 2-NBDLG and 2-NBDG uptake persisted in the absence of Na^+ ion in the extracellular solution (Fig. 3d).

To our surprise, 150 μM of phloretin, a broad spectrum inhibitor against membrane transport including GLUTs/water channels [1, 21], virtually abolished the increase in the fluorescence for

2-NBDLG as well as for 2-NBDG application, leaving only minimally detectable fluorescence ($p < 0.0001$, Fig. 3e). Experiments were performed in quadruplicate and similar results were obtained. It is unlikely that the 2-NBDLG fluorescence was produced by fluorophore NBD, since the fluorescence of MIN6 cells was barely detectable when subjected to KRB containing either NBD-NH_2 or NBD-OH (data not shown).

Cellular heterogeneity in spheroids revealed by a combined use of 2-NBDLG and 2-TRLG

Tumor cells might internalize a wide variety of compounds if exposed for many minutes [22, 23]. To evaluate an occurrence of non-specific uptake, the second L-glucose derivative 2-TRLG [17] was applied simultaneously with 2-NBDLG (Fig. 4 and Online Resource 1). 2-TRLG is a unique "membrane-impermeable" L-glucose derivative bearing Texas Red emitting red fluorescence [17]. As illustrated, combined administration of 2-NBDLG (100 μM) and 2-TRLG (20 μM) for 3 minutes to well-developed MIN6 spheroids (12 DIV) revealed spatially and temporally heterogeneous uptake among cells (Fig. 4). At 2 minutes after starting washout of the tracers, cells located in the central core of the spheroids turned yellow in merged image (Fig. 4e), indicating massive entrance of 2-NBDLG and 2-TRLG (Fig. 4b,c). However, most these cells had lost the yellow color by 4 minutes after washout (Fig. 4k) due to a rapid exit of 2-NBDLG (Fig. 4h), while maintaining 2-TRLG intracellularly (Fig. 4i).

On the other hand, considerable number of cells in the area surrounding the central core showed varied strength of green fluorescence, which well persisted at 4 minutes after washout (Fig. 4b,h, see Online Resource 5). The spatial distribution of such green cells largely overlapped with the area containing cells bearing only weakly-DAPI-positive nuclei (Fig. 4a,g,f and l), and with non-apoptotic/non-necrotic region (Online Resource 7), suggesting that such 2-NBDLG-positive/2-TRLG-negative cells represent viable cells.

Cells showing pale red, deep red, and yellow color were distinguished in the surrounding area at 2 minutes (Fig. 4e). These fluorescent colors can be used as a measure reflecting loss of membrane integrity from severe to less severe in this order, and indeed, some deep red cells lost their color at 4 minutes. Dark quiescent cells were found in peri-central region, which took up little 2-NBDLG as if they were normal cells (Fig. 4e,k). Similar cells could be found as well when D-glucose derivative 2-NBDG was applied similarly with 2-TRLG, appeared less prominent though (Online Resource 6). Further quantification of such dark cells was not conducted in the present study, because only a small portion of tight and thick MIN6 spheroids demonstrated such typical profile of uptake.

DISCUSSION

In the present study, we have shown that a small portion of insulin-secreting clonal cells (MIN6) took up abundant 2-NBDLG when they formed three-dimensional, multi-cellular spheroids exhibiting heterogeneous nuclei at a late culture stage. The 2-NBDLG uptake occurred specifically in a phloretin-inhibitable manner. A combined use of 2-NBDLG with a membrane-impermeable, red fluorescence-emitting L-glucose derivative 2-TRLG provides a unique method for visualizing heterogeneity of tumor cells in multiple colors.

Characterization of tumor cells by fluorescent L-glucose derivatives

Noticeable uptake of 2-NBDLG proceeded along with formation of three-dimensional spheroids, consisting of cells bearing nuclei of heterogeneous size accompanied by DAPI-positive fibrous processes in some cases. Such features are among major cytological criteria in clinical diagnosis for tumor cells suspected of high grade of malignancy.

Multi-cellular spheroids are thought to emulate the cellular heterogeneity in tumor typically found in the body cavity fluid and in solid tumors [24, 25]. In such three-dimensionally grown tumor, there are cells in intermediate states between perfectly healthy and totally collapsed, due to insufficient oxygen/fuel supply and metabolite clearance, pharmacological treatment, and inflammatory response.

The existence of such intermediate cells makes it often difficult to characterize tumor cells by using functional probes such as 2-NBDG/2-NBDLG.

2-TRLG can be used as a sensitive measure for the membrane state. Once 2-TRLG entered into the cytosol of such intermediate cells, it remained intracellularly for tens of minutes, whereas it disappeared soon when permeated into totally collapsed cells (Fig. 4). Since a more hydrophilic analogue of 2-TRLG failed to show such characteristics (data not shown), charged lipophilic property of 2-TRLG might well be related to the retention. Such unique feature of 2-TRLG is useful for recognizing partially damaged cells during live imaging, contrasted to a commercially available dead cell marker such as propidium iodide, which irreversibly binds to the nucleus once entering into cells (Online Resource 7).

Interestingly, there were cells sustaining 2-NBDLG fluorescence for over 30 minutes as well as dark and quiescent cells in the area surrounding the necrotic central core of spheroids. Questions are posed what the difference between 2-NBDLG-positive and negative cells is, and whether 2-NBDLG is metabolized after entering into tumor cells.

Mechanistic consideration underlying 2-NBDLG uptake into tumor cells

From the fact that neither cytochalasin B nor a large amount of D-glucose could totally abolish the uptake of 2-NBDLG and of 2-NBDG, it may be speculated that MIN6 insulinoma expresses phloretin-sensitive, but non-GLUT, non-stereoselective pathways when forming multi-cellular

spheroids. Glucose entry into cells might well occur not only through saturable (carrier-mediated) processes requiring glucose binding to the postulated recognition site of the transporter like GLUTs [26, 27] but also through non-saturable ones. Indeed, use of 2-NBDG has suggested in some plant cells that a mercury-sensitive, water-channel-like mechanisms operate concomitantly with saturable processes [28]. 2-NBDLG uptake into MIN6 cells was virtually abolished by phloretin, which is the aglycone of phlorizin, a phytoalexin produced by such as apple and cherry trees. Phloretin, being used as a GLUT inhibitor for many years, is also known as a potent inhibitor of aquaporins [21]. Thus, it is of interest to examine if such channel-like processes participate in the glucose transport in insulinoma cells [21, 29].

A large amount of 4,6-*O*-ethylidene-D-glucose has been used by some investigators as a competitive inhibitor against GLUT-mediated 2-NBDG transport, postulating that it selectively interacts with the outward-facing sugar binding site of a carrier [9]. However, 4,6-*O*-ethylidene-D-glucose might not fully reflect the stereoselective property of D-glucose, since its mirror image isomer also significantly inhibited 2-NBDG uptake into MIN6 cells (data not shown).

Clinical significance of the uptake of fluorescent L-glucose derivatives

Evidence has been accumulated which shows that 2-NBDG is taken up into variety of tumor cell lines, such as derived from melanoma, breast, liver, colorectal cancers, and glioma [10, 12, 22, 27]. 2-NBDG has also been used as a contrast agent for imaging biopsy specimen obtained from oral, breast, and

Barrett's esophagus cancer patients [11, 13, 14]. However, critical issues to be solved when using D-glucose derivatives in tumor imaging may include how to reduce the uptake into normal tissues containing fat and muscle, and how to discriminate the uptake into tumor cells from that due to inflammatory and/or non-cancerous anomalies [12, 14]. Difficulty in applying them for diabetic patients may also be pointed out. The least interaction with GLUTs, if any, of L-glucose derivatives like 2-NBDLG would make undesirable binding to non-tumor cells, or toxic effect in other words, minimum compared to that expected when using 2-NBDG.

One of the key therapeutic strategies against rapidly growing tumor would be deprivation of energy source and nutrients [30]. However, tumor cells that survive in low-nutrient environment might well develop regulatory mechanisms enabling utilization of unusual carbohydrate as a carbon source as reported in some lower organisms [31, 32]. Heterogeneous nuclei and tubulin-like fibrous structure are among important features of malignant tumor spheroids [33]. Illuminating the breakdown in the stereoselectivity of tumor cells by their heterogeneous acceptance of unnatural sugar/sugar analogues might serve a new indication for cancer diagnosis eventually at the single cell level and help determining therapies against cancer. Further investigation is required to clarify the transport mechanism, intracellular fate, as well as limitation of 2-NBDLG in tumor imaging.

ACKNOWLEDGEMENTS

This research was supported by Science and Technology Incubation Program in Advanced Regions (KY, TY), Support for Increasing the Value for University Patents (KY), Collaborative Research Based on Industrial Demand (KY), and A-STEP (TY, TT, KY) from JST, Grant-in-Aid for Scientific Research on Priority Areas (KY, 20019003, 20056001), Research Funds from Research Foundation for Opto-Science and Technology (KY), and Grant for Hirosaki University Institutional Research (KY). A part of the present study was seen on a patent pending [WO2012/133688]. The authors thank Drs. Junichi Miyazaki (Osaka Univ.) for providing us MIN6 cells, Sechiko Suga, Seiji Watanabe and Kazuyoshi Hirota (Hirosaki Univ.) for fluorescence measurement, Hideaki Matsuoka (Tokyo Univ. Agri. Technol.), Hirotaka Onoe and Tsuyoshi Tahara (Riken), Iwao Kanno, Kazuto Masamoto, and Yukie Yoshii (National Inst. Radiol. Sci.) for helpful discussion, Masahito Kogawa and Rumiko Narita (Hirosaki Univ.) for technical assistance.

CONFLICT OF INTEREST

KY, TY, and TT received grants above noted from the Japanese government for developing potential cancer diagnostic agents, in which AS, KN, KO and YO are collaborators. KY, TY and TT, and in one case AS and YO, are co-applicants for multiple patents related to cancer diagnostics using

fluorescent L-glucose derivatives. KY, AS, and KO assigned ownership of all these patents to Hirosaki University.

REFERENCES AND NOTES

1) Zhao FQ, Keating AF. Functional properties and genomics of glucose transporters. Curr Genomics. 2007; 8:113-28.

2) Yoshioka K, Takahashi H, Homma T, et al. A novel fluorescent derivative of glucose applicable to the assessment of glucose uptake activity of Escherichia coli. Biochim Biophys Acta. 1996; 1289:5-9.

3) Yamada K, Nakata M, Horimoto N, Saito M, Matsuoka H, Inagaki N. Measurement of glucose uptake and intracellular calcium concentration in single, living pancreatic beta-cells. J Biol Chem. 2000; 275:22278-83.

4) Yamada K, Saito M, Matsuoka H, Inagaki N. A real-time method of imaging glucose uptake in single, living mammalian cells. Nat Protoc. 2007; 2:753-62.

5) Ohtsubo K, Takamatsu S, Minowa MT, Yoshida A, Takeuchi M, Marth JD. Dietary and genetic control of glucose transporter 2 glycosylation promotes insulin secretion in suppressing diabetes. Cell. 2005; 123:1307-21.

6) Bernardinelli Y, Magistretti PJ, Chatton JY. Astrocytes generate Na+-mediated metabolic waves. Proc Natl Acad Sci U S A. 2004; 101:14937-42.

7) Rouach N, Koulakoff A, Abudara V, Willecke K, Giaume C. Astroglial metabolic networks sustain hippocampal synaptic transmission. Science. 2008; 322:1551-5.

8) Gandhi GK, Cruz NF, Ball KK, Theus SA, Dienel GA. Selective astrocytic gap junctional trafficking of molecules involved in the glycolytic pathway: impact on cellular brain imaging. J Neurochem. 2009; 110:857-69.

9) Barros LF, Courjaret R, Jakoby P, Loaiza A, Lohr C, Deitmer JW. Preferential transport and metabolism of glucose in Bergmann glia over Purkinje cells: a multiphoton study of cerebellar slices. Glia. 2009; 57:962-70.

10) O'Neil RG, Wu L, Mullani N. Uptake of a fluorescent deoxyglucose analog (2-NBDG) in tumor cells. Mol Imaging Biol. 2005; 7:388-92.

11) Nitin N, Carlson AL, Muldoon T, El-Naggar AK, Gillenwater A, Richards-Kortum R. Molecular imaging of glucose uptake in oral neoplasia following topical application of fluorescently labeled deoxy-glucose. Int J Cancer. 2009; 124:2634-42.

12) Sheth RA, Josephson L, Mahmood U. Evaluation and clinically relevant applications of a fluorescent imaging analog to fluorodeoxyglucose positron emission tomography. J Biomed Opt. 2009; 14:064014.

13) Langsner RJ, Middleton LP, Sun J, et al. Wide-field imaging of fluorescent deoxy-glucose in ex vivo malignant and normal breast tissue. Biomed Opt Express. 2011; 2:1514-23.

14) Thekkek N, Maru DM, Polydorides AD, Bhutani MS, Anandasabapathy S, Richards-Kortum R. Pre-clinical evaluation of fluorescent deoxyglucose as a topical contrast agent for the detection of

Barrett's-associated neoplasia during confocal imaging. Technol Cancer Res Treat. 2011; 10:431-41.

15) Viale A, Pettazzoni P, Lyssiotis CA, et al. Oncogene ablation-resistant pancreatic cancer cells depend on mitochondrial function. Nature. 2014; 514:628-32.

16) Yamamoto T, Nishiuchi Y, Teshima T, Matsuoka H, Yamada K. Synthesis of 2-NBDLG, a fluorescent derivative of L-glucosamine; the antipode of D-glucose tracer 2-NBDG. Tetrahedron Lett. 2008; 49:6876-8.

17) Yamamoto T, Tanaka S, Suga S, et al. Syntheses of 2-NBDG analogues for monitoring stereoselective uptake of D-glucose. Bioorg Med Chem Lett. 2011; 21:4088-96.

18) Miyazaki J, Araki K, Yamato E, et al. Establishment of a pancreatic beta cell line that retains glucose-inducible insulin secretion: special reference to expression of glucose transporter isoforms. Endocrinology. 1990; 127:126-32.

19) O'Driscoll L, Gammell P, McKiernan E, et al. Phenotypic and global gene expression profile changes between low passage and high passage MIN-6 cells. J Endocrinol. 2006; 191:665-76.

20) Bonne D, Heusele C, Simon C, Pantaloni D. 4',6-Diamidino-2-phenylindole, a fluorescent probe for tubulin and microtubules. J Biol Chem. 1985; 260:2819-25.

21) Tsukaguchi H, Shayakul C, Berger UV, et al. Molecular characterization of a broad selectivity neutral solute channel. J Biol Chem. 1998; 273:24737-43.

22) Cheng Z, Levi J, Xiong Z, et al. Near-infrared fluorescent deoxyglucose analogue for tumor optical imaging in cell culture and living mice. Bioconjug Chem. 2006; 17:662-9.

23) Kelf TA, Sreenivasan VK, Sun J, Kim EJ, Goldys EM, Zvyagin AV. Non-specific cellular uptake of surface-functionalized quantum dots. Nanotechnology. 2010; 21:285105.

24) Pampaloni F, Reynaud EG, Stelzer EH. The third dimension bridges the gap between cell culture and live tissue. Nat Rev Mol Cell Biol. 2007; 8:839-45.

25) Elliott NT, Yuan F. A review of three-dimensional in vitro tissue models for drug discovery and transport studies. J Pharm Sci. 2011; 100:59-74.

26) Lefevre PG. Sugar transport in the red blood cell: structure-activity relationships in substrates and antagonists. Pharmacol Rev. 1961; 13:39-70.

27) Deng D, Xu C, Sun P, et al. Crystal structure of the human glucose transporter GLUT1. Nature. 2014; 510:121-5.

28) Conde C, Silva P, Agasse A, Tavares RM, Delrot S, Geros H. An Hg-sensitive channel mediates the diffusional component of glucose transport in olive cells. Biochim Biophys Acta. 2007; 1768:2801-11.

29) Delporte C, Virreira M, Crutzen R, et al. Functional role of aquaglyceroporin 7 expression in the pancreatic beta-cell line BRIN-BD11. J Cell Physiol. 2009; 221:424-9.

30) Cairns RA, Harris IS, Mak TW. Regulation of cancer cell metabolism. Nat Rev Cancer. 2011; 11:85-95.

31) Sasajima KI, Sinskey AJ. Oxidation of L-glucose by a pseudomonad. Biochim Biophys Acta. 1979; 571:120-6.

32) Shimizu T, Takaya N, Nakamura A. An L-glucose catabolic pathway in Paracoccus species 43P. J Biol Chem. 2012; 287:40448-56.

33) McCarroll JA, Gan PP, Erlich RB, et al. TUBB3/betaIII-tubulin acts through the PTEN/AKT signaling axis to promote tumorigenesis and anoikis resistance in non-small cell lung cancer. Cancer Res. 2015; 75:415-25.

FIGURE LEGENDS

Fig. 1 Representative images of MIN6 cell spheroids subjected to a brief application of solution containing either 2-NBDG (a-d) or 2-NBDLG (e-h) at 6 days *in vitro* (DIV). **a**, Differential interference contrast (DIC) image. **b**, Autofluorescence before application of the fluorescent tracer. **c**, During application of 100 μM of 2-NBDG-containing solution for 3 minutes. **d**, Fluorescence image taken at 4 minutes after starting washout of the tracer. 2-NBDG uptake varied considerably from prominent (arrow) to minimal (asterisk) among cells. **e-h**, Similar to a-d, but for application of 100 μM of 2-NBDLG to the same series of culture examined on the same day. The uptake of 2-NBDLG into MIN6 cells at this stage was very weak, although some cells showed faint fluorescence (asterisks). Scale bar is common to all images.

Fig. 2 Uptake of 2-NBDLG into MIN6 cells forming spheroids. **a**, DIC image of MIN6 cells at 11 DIV. **b**, Autofluorescence measured before application of 100 μM of 2-NBDLG for 3 min. **c**, During application of 2-NBDLG. Note that both spheroids (A and B) were evenly superfused by 2-NBDLG solution. **d**, Two minutes after starting washout of the 2-NBDLG solution. Cells in the upper spheroid (A) exhibited a strong 2-NBDLG fluorescence in the cytosol, whereas only a minimum increase in the fluorescence was seen in cells in the lower spheroid (B). **e**, Live-cell nuclear staining by DAPI, conducted after finishing 2-NBDLG application. Upper spheroid contained cells having extremely DAPI-positive large nucleus (A), whereas lower one showed nuclei of normal size. **f**, Merged image of

d and e. Multi-stack z-sections of DAPI staining are available in Online Resource 4 in detail. Asterisks indicate cells moderately positive for 2-NBDLG in other spheroids. Scale bar is common to all panels.

Fig. 3 Quantitative evaluation of the 2-NBDG and 2-NBDLG uptake into MIN6 cells examined at 10-13 DIV. **a**, Changes in the fluorescence of MIN6 cells subjected to 2-NBDG or 2-NBDLG solution. **b**, The net increase in the fluorescence in (a). **c**, Increase in the fluorescence in the absence or presence of a GLUT inhibitor cytochalasin B (10 μM, CB). **d**, Effect of Na^+-free condition on the 2-NBDG and 2-NBDLG uptake. **e**, Effect of phloretin (150 μM, PHT) on the 2-NBDG and 2-NBDLG uptake. Values are expressed as mean percent increase in the fluorescence relative to the fluorescence increase for 2-NBDG application on the same 96-well plate (b-e). Values in individual columns represent mean fluorescence of more than 12 ROIs (more than 5000 cells are included in each ROI) and expressed as mean ± S.D.

Fig. 4 Confocal microscopic images of 12 DIV MIN6 spheroids subjected to 100 μM of 2-NBDLG (green) and 20 μM of 2-TRLG (red) mixture for 3 minutes followed by washout. **a**, Nuclear staining with DAPI in live cell condition. The central core region of spheroids appears to be necrotic (see also d). **b** and **c**, Fluorescence images taken at 2 minutes after starting washout of the tracers in the green (b, 500-580 nm) and the red (c, 580-740 nm) channel, reflecting entrance of 2-NBDLG and 2-TRLG, respectively. **d**, Differential interference contrast (DIC) image. **e**, Overlay of the green, red, and DIC images. **f**, Overlay of (a) and (e). Cellular heterogeneity is clearly seen by a combination of the two

fluorescent colors. Cells indicated by arrows exhibited yellow color at 2 minutes (e), turned red at 4 minutes (k). This is because green 2-NBDLG was lost (b, h), while red 2-TRLG remained (c, i). If one saw a single 2-NBDLG image (b), cells indicated by arrows would have been misinterpreted to be similar to cells nearby. **g-l**, Similar to a-f, but images taken at 4 minutes after starting washout. Numbers of green cells with no red fluorescence, seen in the area surrounding the central core, preserved their color for at least up to 30 minutes (h, i, k). Also noted are dark cells in the area just surrounding the central core (b, e, h, k). Bars are common to all panels.

Fig. 1

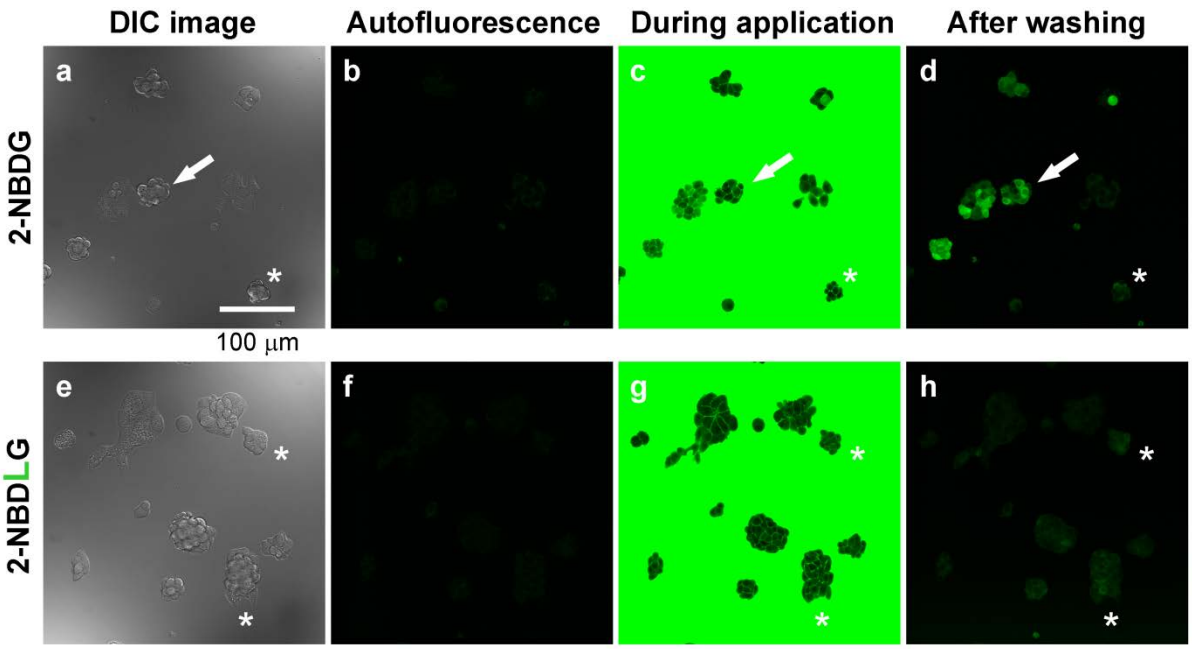
DIC image
Autofluorescence
During application
After washing
2-NBDG
2-NBDLG
a
b
c
d
e
f
g
h
100 μm

Fig. 2

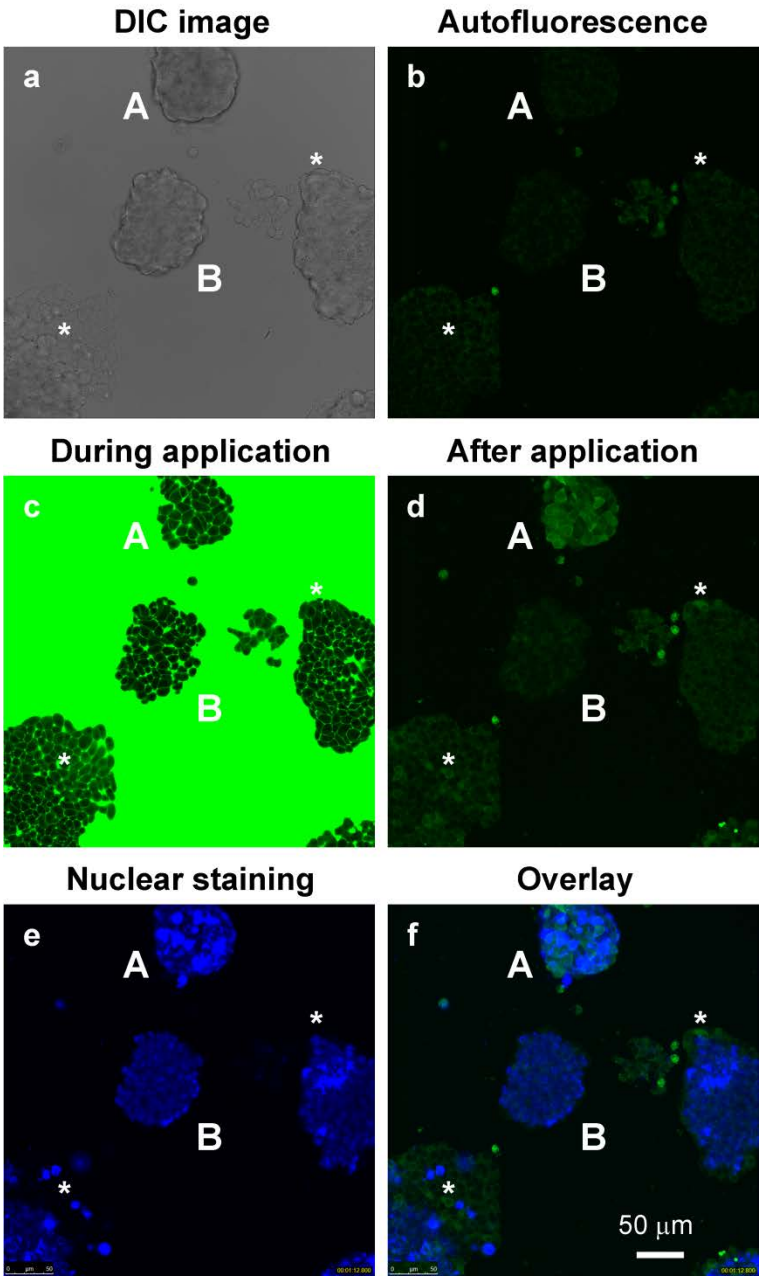
DIC image
Autofluorescence
a
b
A
B
*
During application
After application
c
d
Nuclear staining
Overlay
e
f
50 µm

Fig. 3

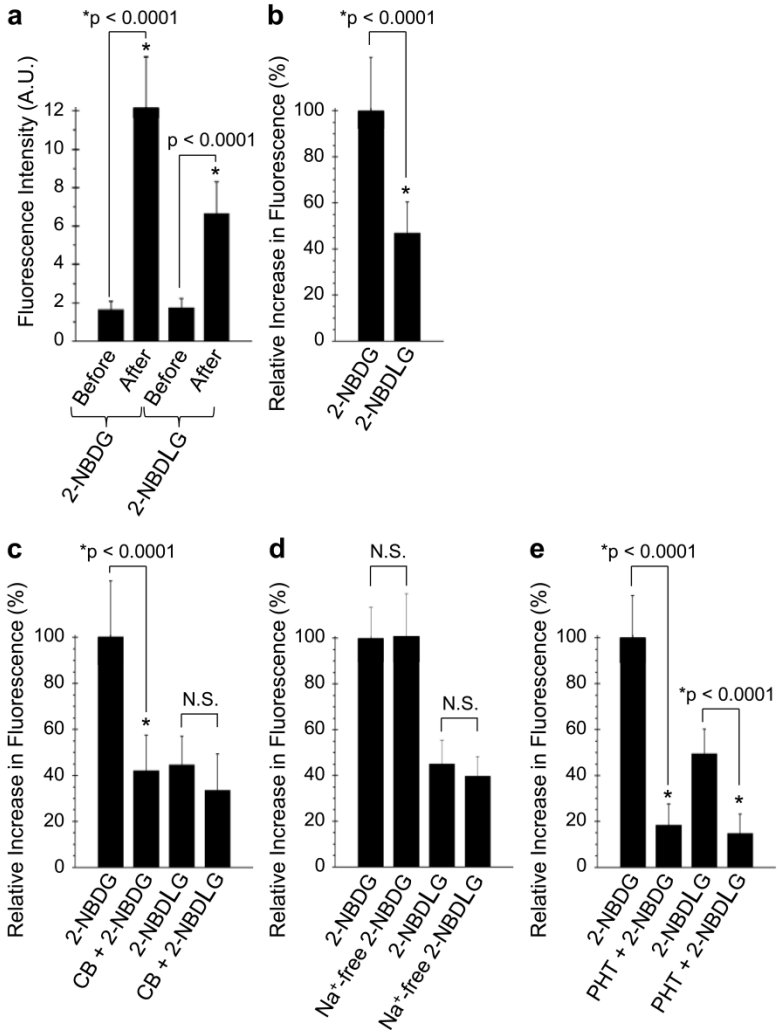
a
*p < 0.0001
p < 0.0001
Fluorescence Intensity (A.U.)
0
2
4
6
8
10
12
Before
After
Before
After
2-NBDG
2-NBDLG
b
*p < 0.0001
Relative Increase in Fluorescence (%)
0
20
40
60
80
100
2-NBDG
2-NBDLG
c
*p < 0.0001
N.S.
Relative Increase in Fluorescence (%)
0
20
40
60
80
100
2-NBDG
CB + 2-NBDG
2-NBDLG
CB + 2-NBDLG
d
N.S.
N.S.
Relative Increase in Fluorescence (%)
0
20
40
60
80
100
2-NBDG
Na+-free 2-NBDG
2-NBDLG
Na+-free 2-NBDLG
e
*p < 0.0001
*p < 0.0001
Relative Increase in Fluorescence (%)
0
20
40
60
80
100
2-NBDG
PHT + 2-NBDG
2-NBDLG
PHT + 2-NBDLG

Fig. 4

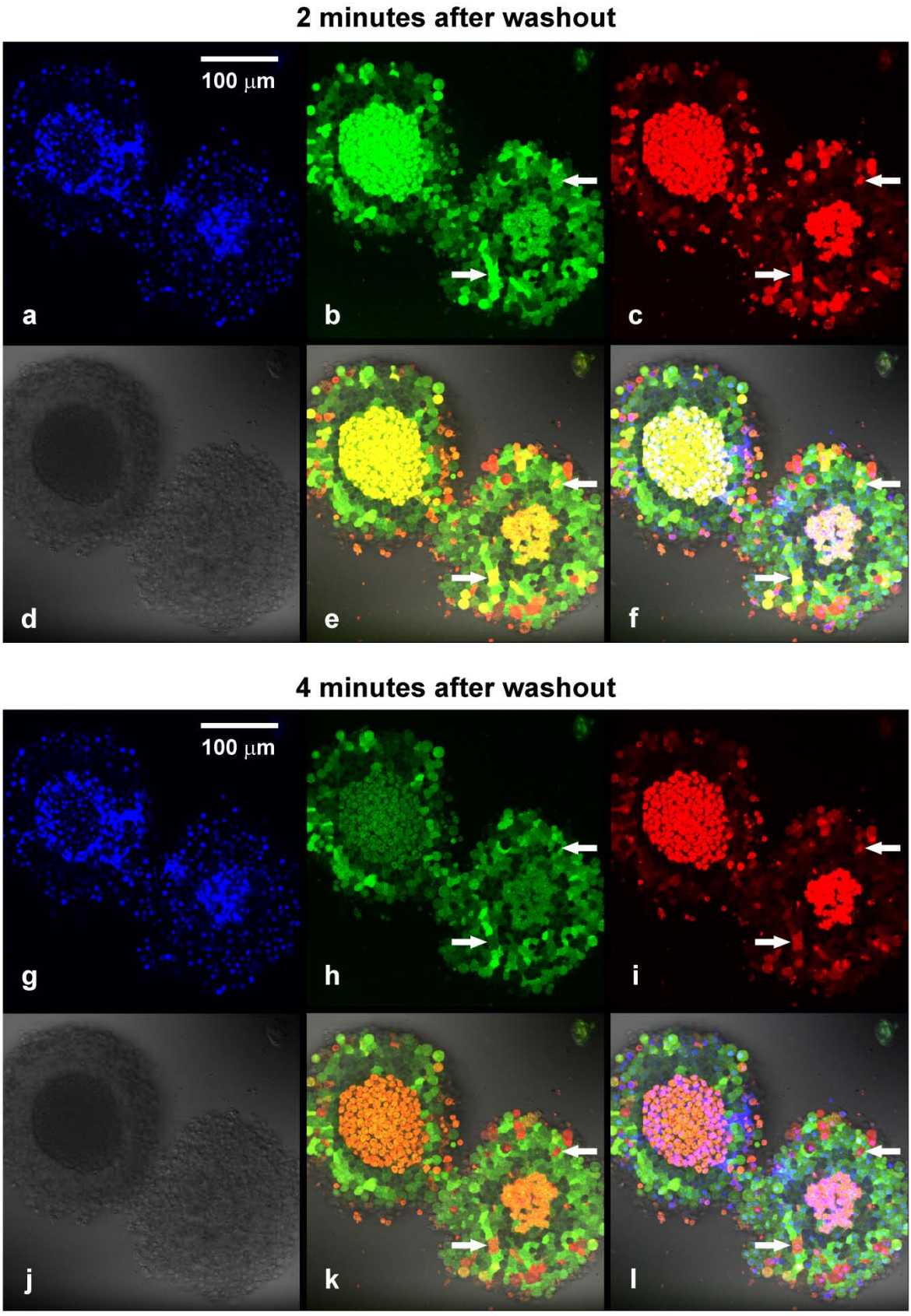
2 minutes after washout
100 μm
a
b
c
d
e
f
4 minutes after washout
100 μm
g
h
i
j
k
l

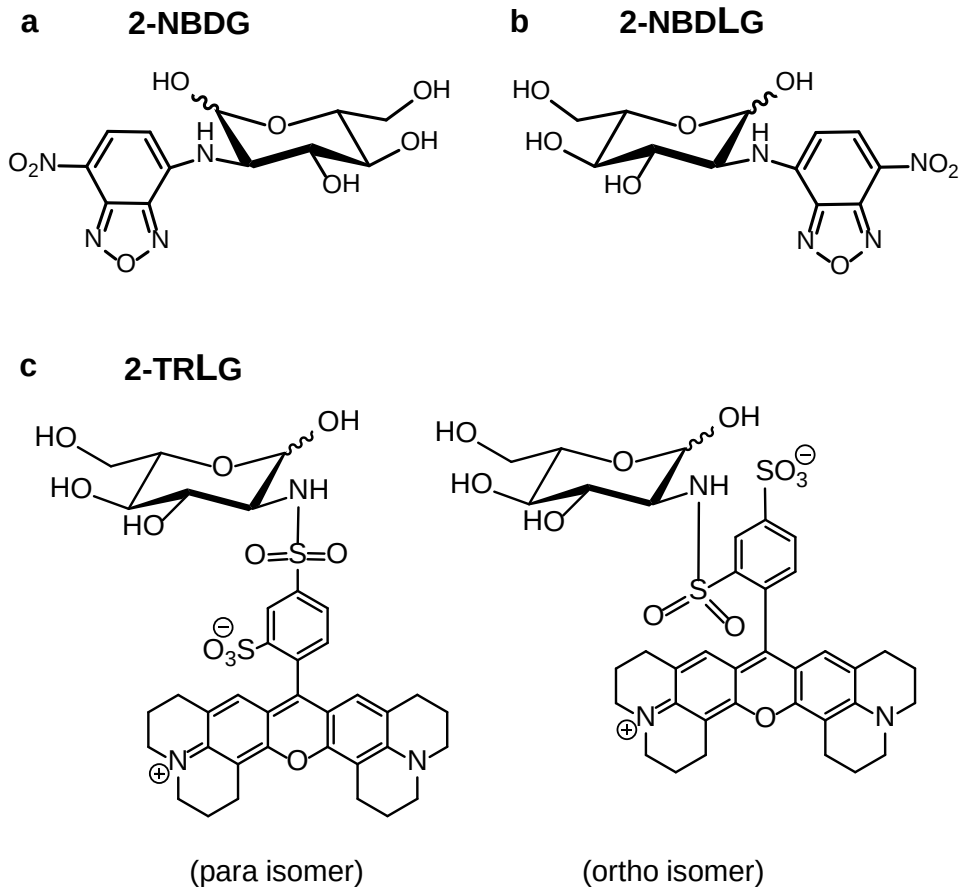

Online Resource 1. Chemical structures of 2-NBDG (a), 2-NBDLG (b), and 2-TRLG (c), respectively.

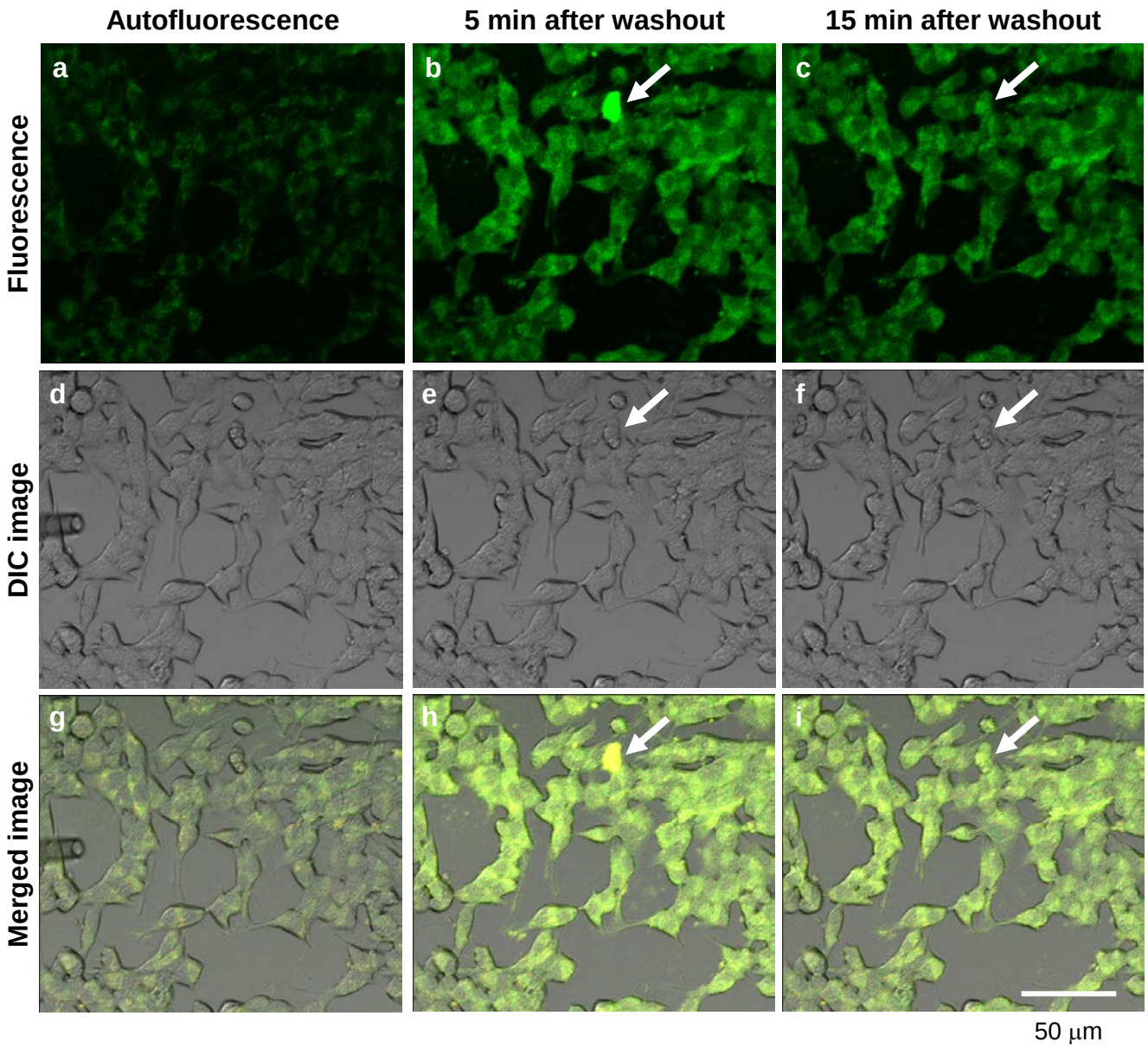

Online Resource 2. Typical uptake of 2-NBDG into two-dimensionally spreading MIN6 cells (passages, possibly over 40 times). Representative fluorescence images (a-c), differential interference contrast (DIC) images (d-f), and merged images (g-i) are shown. **a**, Autofluorescence before application of 200 μM of 2-NBDG for 1 minute. **b** and **c**, Fluorescence images taken at 5 minutes and 15 minutes after starting washout of 2-NBDG solution, respectively. Note that most cells exhibit homogeneous fluorescence except for a cell indicated by an arrow, which showed a strong fluorescence at 5 minutes, and lost the fluorescence intensity at 15 minutes, possibly by leaking out of 2-NBDG due to a loss of membrane integrity. A glass pipette seen in the left was used to apply the fluorescent tracer in this experiment.

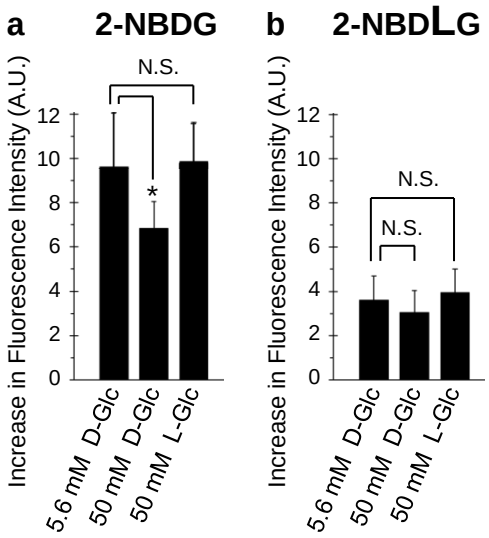

Online Resource 3. Effect of a large amount of D- or L-glucose on the uptake of 2-NBDG (a) and 2-NBDLG (b) into MIN6 cells examined at 10-12 DIV. **a**, 2-NBDG uptake expressed as the increase in fluorescence intensity was reduced only moderately by 50 mM of D-glucose ($p < 0.0001$), and no reduction was detected by the same amount of L-glucose. Experiments were performed in triplicate, and the mean increase in the fluorescence for 2-NBDG application in the presence of either 50 mM of D- or L-glucose to that in control solution containing 5.6 mM of D-glucose were 70.9 ± 0.2 % or 104.2 ± 2.3 %, respectively. **b**, Similar to (a), but for 2-NBDLG application. The uptake of 2-NBDLG was attenuated only slightly by 50 mM of D-glucose, while majority of the fluorescence remained (81.5 ± 7.2 % in average) in experiments performed in septuplicate. No significant change in 2-NBDLG uptake on the same plates was detected by 50 mM of L-glucose (102.1 ± 3.6 %). Values represent mean fluorescence of more than 33 ROIs, and are expressed as mean ± S.D.

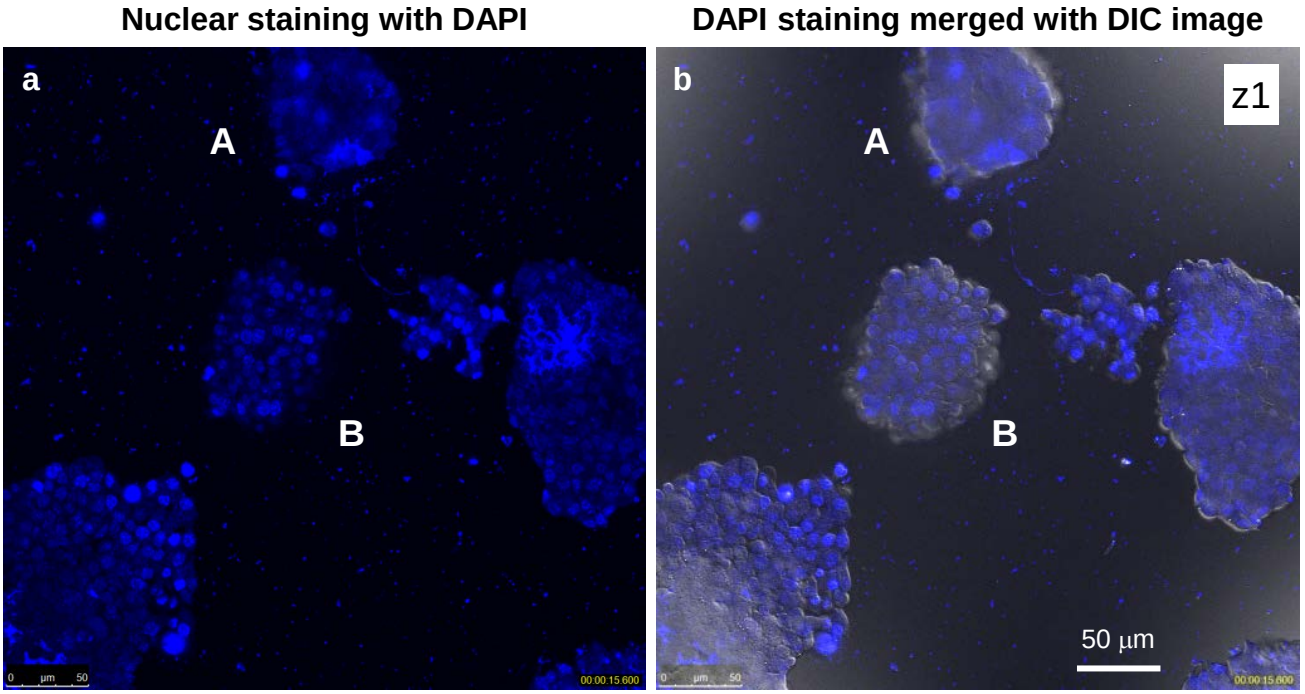

Online Resource 4-1. Serial DAPI and DIC images (z-stack) for Figure 2. The number in the upper-right corner indicates z position, which was numbered consecutively from the cover slip surface every 6 microns. **a**, DAPI staining. **b**, Overlay of DAPI and DIC images. Application of DAPI was done for living cells at 37ºC for an hour (see text). Spheroid A is characterized by strongly DAPI-positive large nuclei (see z2-z5), whereas spheroid B consisted of cells having minimally stained nuclei of ordinary size (see z3-z6) except for necrotic cells (z1 and z2). Scale bar is common to all panels.

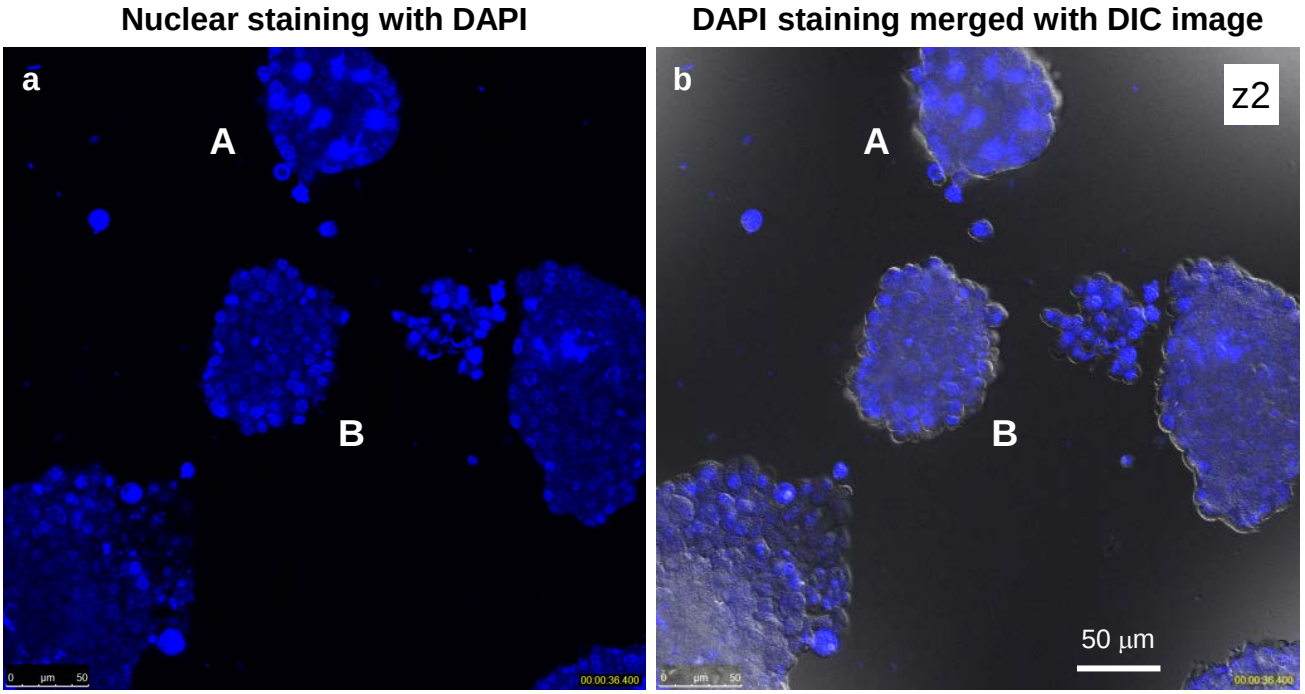

Online Resource 4-2. Similar to Online Resource 4-1, but image taken at 6 microns above.

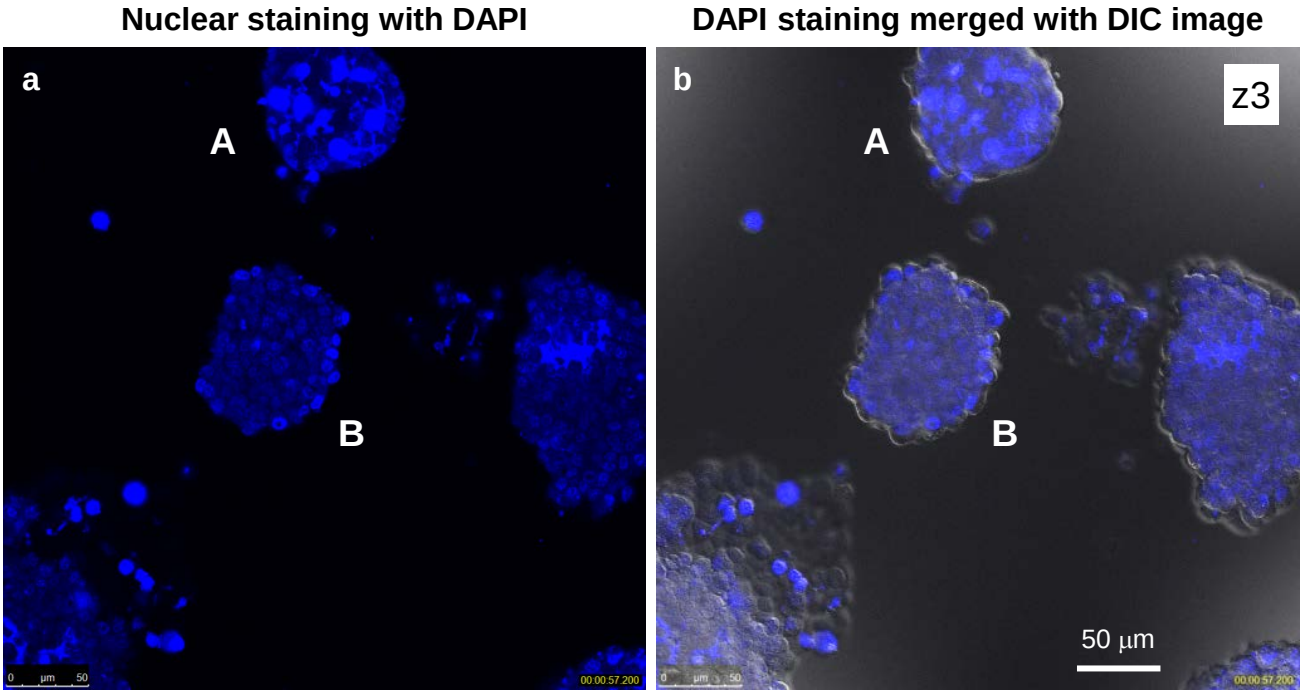

Online Resource 4-3. Similar to Online Resource 4-1, but image taken at 12 microns above.

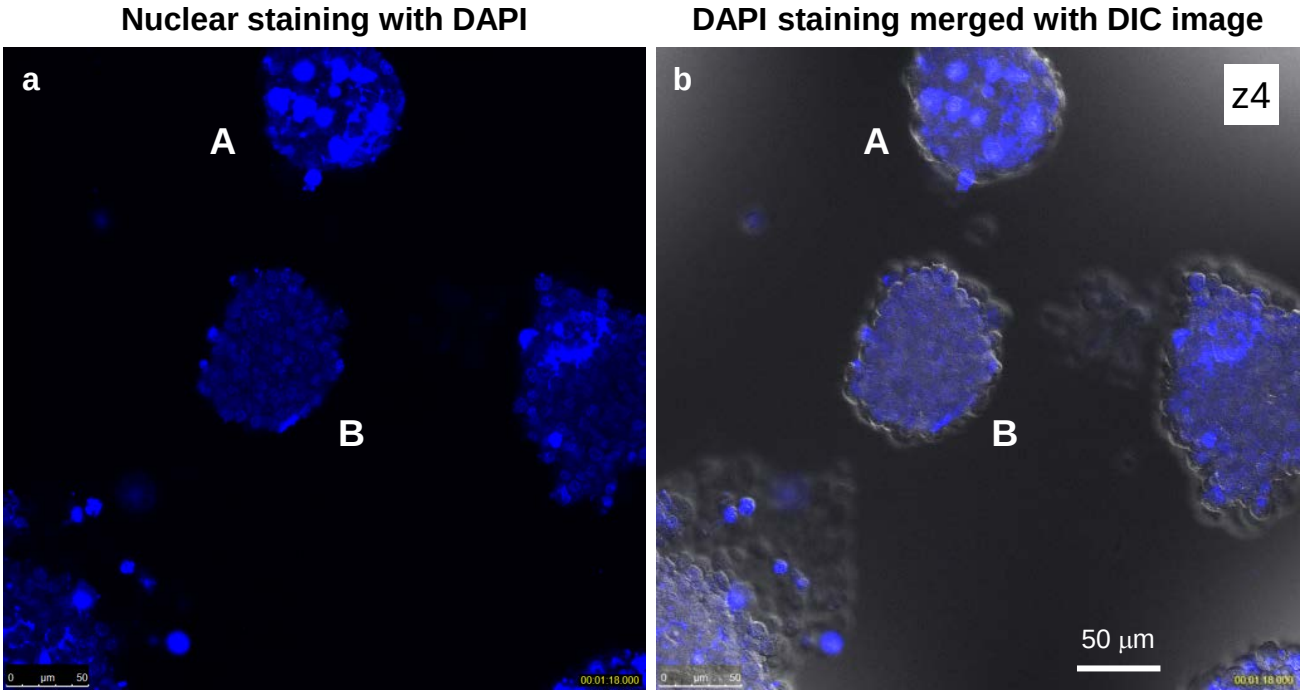

Online Resource 4-4. Similar to Online Resource 4-1, but image taken at 18 microns above.

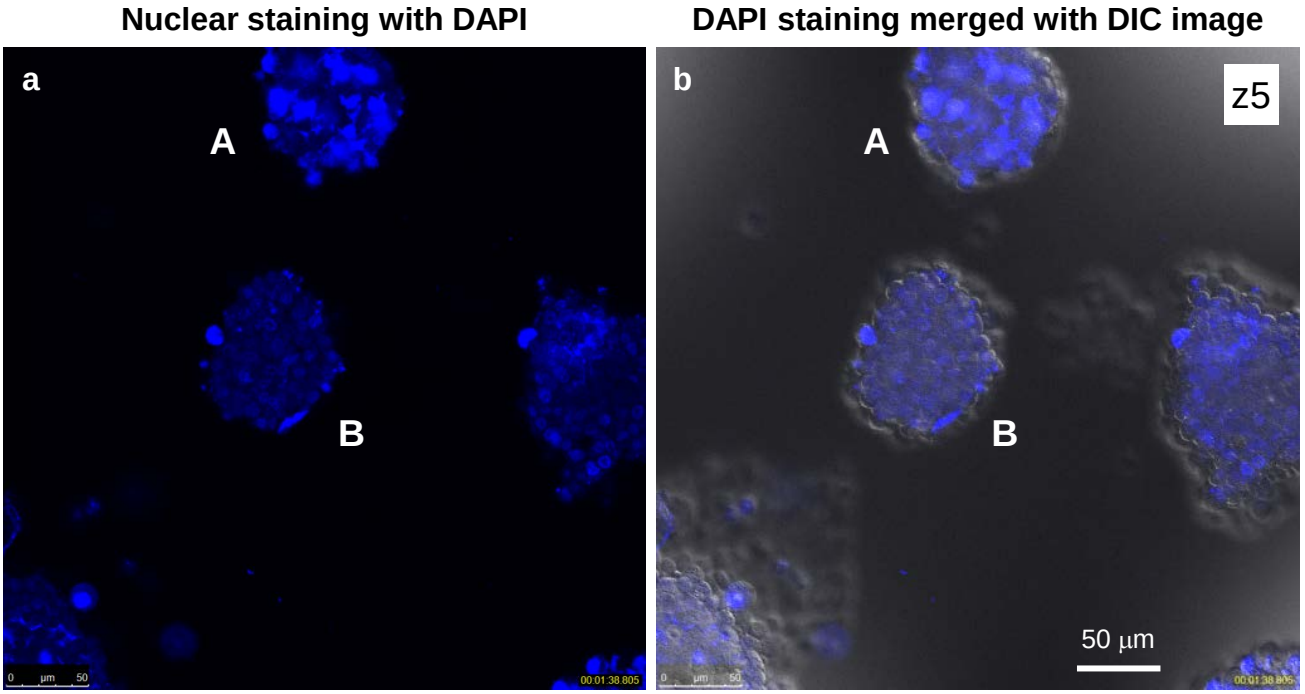

Online Resource 4-5. Similar to Online Resource 4-1, but image taken at 24 microns above.

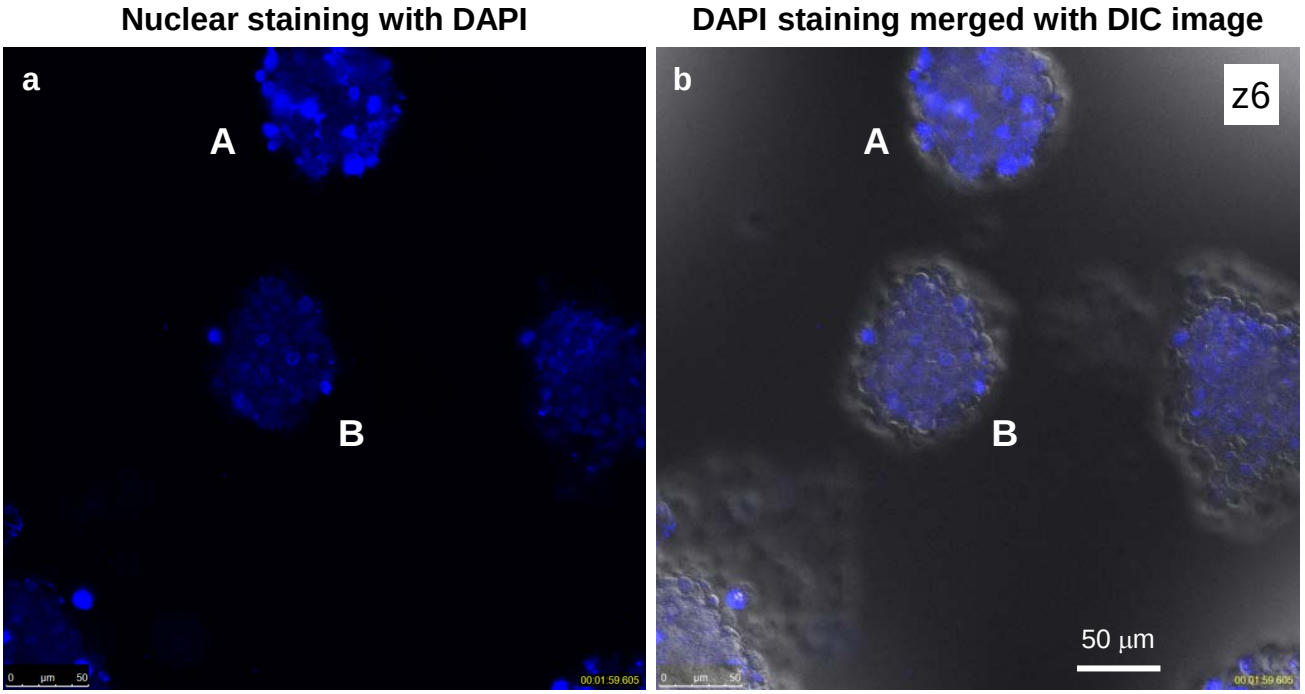

Online Resource 4-6. Similar to Online Resource 4-1, but image taken at 30 microns above.

Online Resource 5-1. Confocal microscopic images of 12 DIV MIN6 spheroids taken before starting the fluorescent tracer application, in three representative z sections. **a-f**, Pictures taken at the bottom part of the spheroid. **a**, Nuclear staining with DAPI in live cell condition. **b** and **c**, Fluorescence images taken in the green (b, 500-580 nm) and the red (c, 580-740 nm) wavelength range, reflecting entrance of 2-NBDLG and 2-TRLG, respectively. **d**, DIC image. **e**, Overlay of the green, red, and DIC images. **f**, Overlay of DAPI image and (e). **g-l**, and **m-r**, Similar to a-f, but images taken at 8 and 16 microns above, respectively. Bars are common to all panels.

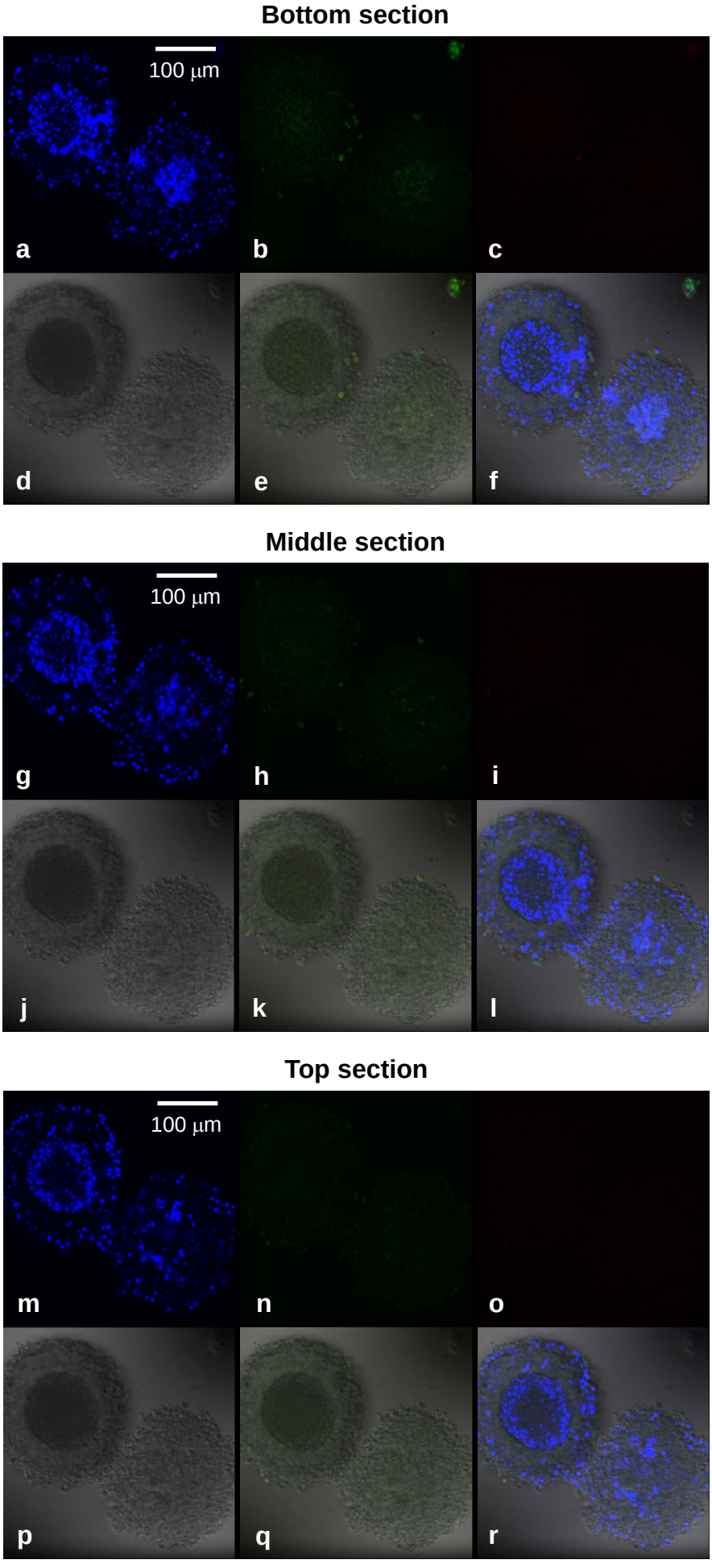

Online Resource 5-2. **S**imilar to Online Resource 5-1, but taken at 2 minutes after starting washout of 100 μM of 2-NBDLG (green) and 20 μM of 2-TRLG (red) mixture, in three representative z sections. **a-f**, Pictures taken at the bottom part of the spheroid. **a**, Nuclear staining with DAPI in live cell condition. **b** and **c**, Fluorescence images taken in the green (b, 500-580 nm) and the red (c, 580-740 nm) wavelength range, reflecting entrance of 2-NBDLG and 2-TRLG, respectively. **d**, DIC image. **e**, Overlay of the green, red, and DIC images. **f**, Overlay of DAPI image and (e). **g-l**, and **m-r**, Similar to a-f, but images taken at 8 and 16 microns above, respectively. Bars are common to all panels.

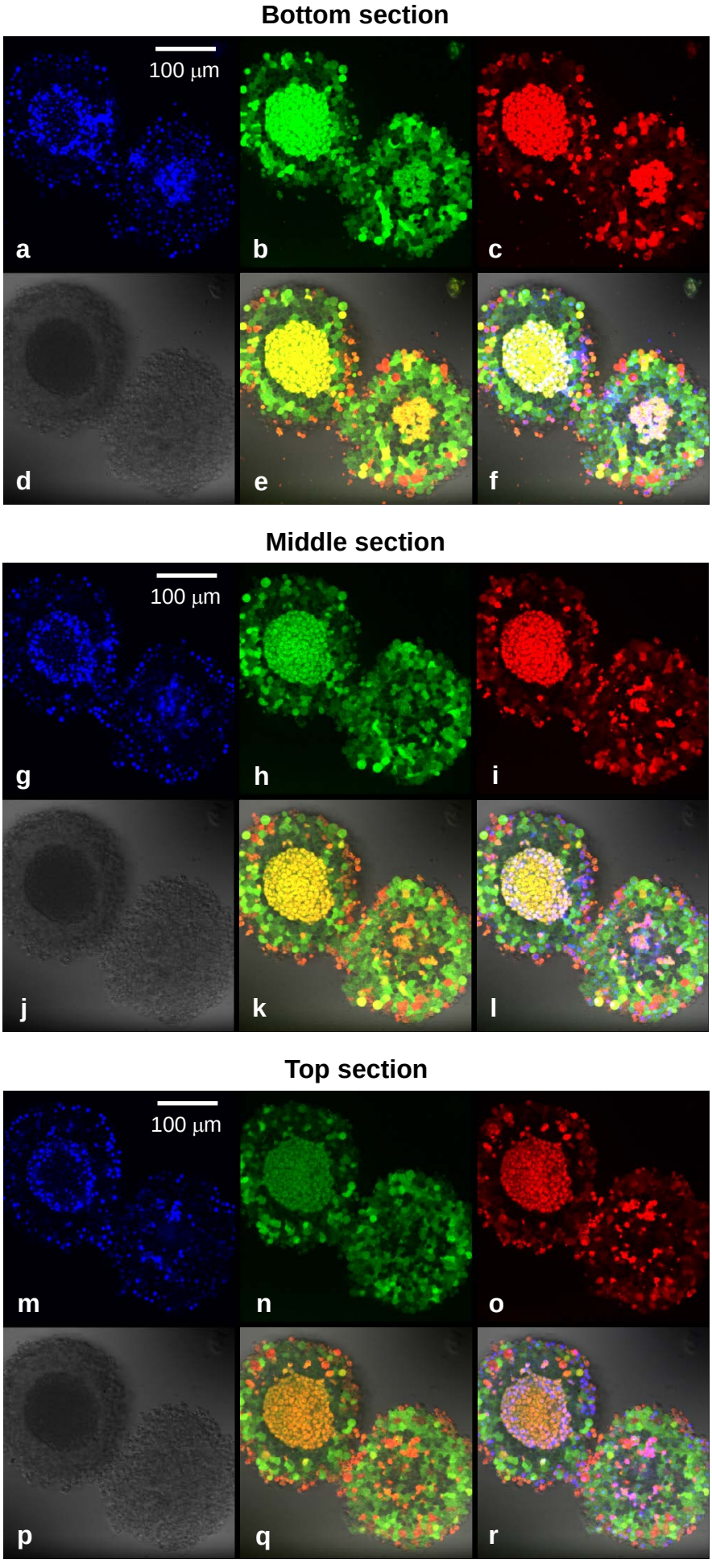

Online Resource 5-3. Similar to Online Resource 5-1, but taken at 4 minutes after starting washout of 100 μM of 2-NBDLG (green) and 20 μM of 2-TRLG (red) mixture, in three representative z sections. **a-f**, Pictures taken at the bottom part of the spheroid. **a**, Nuclear staining with DAPI in live cell condition. **b** and **c**, Fluorescence images taken in the green (b, 500-580 nm) and the red (c, 580-740 nm) wavelength range, reflecting entrance of 2-NBDLG and 2-TRLG, respectively. **d**, DIC image. **e**, Overlay of the green, red, and DIC images. **f**, Overlay of DAPI image and (e). **g-l**, and **m-r**, Similar to a-f, but images taken at 8 and 16 microns above, respectively. Bars are common to all panels.

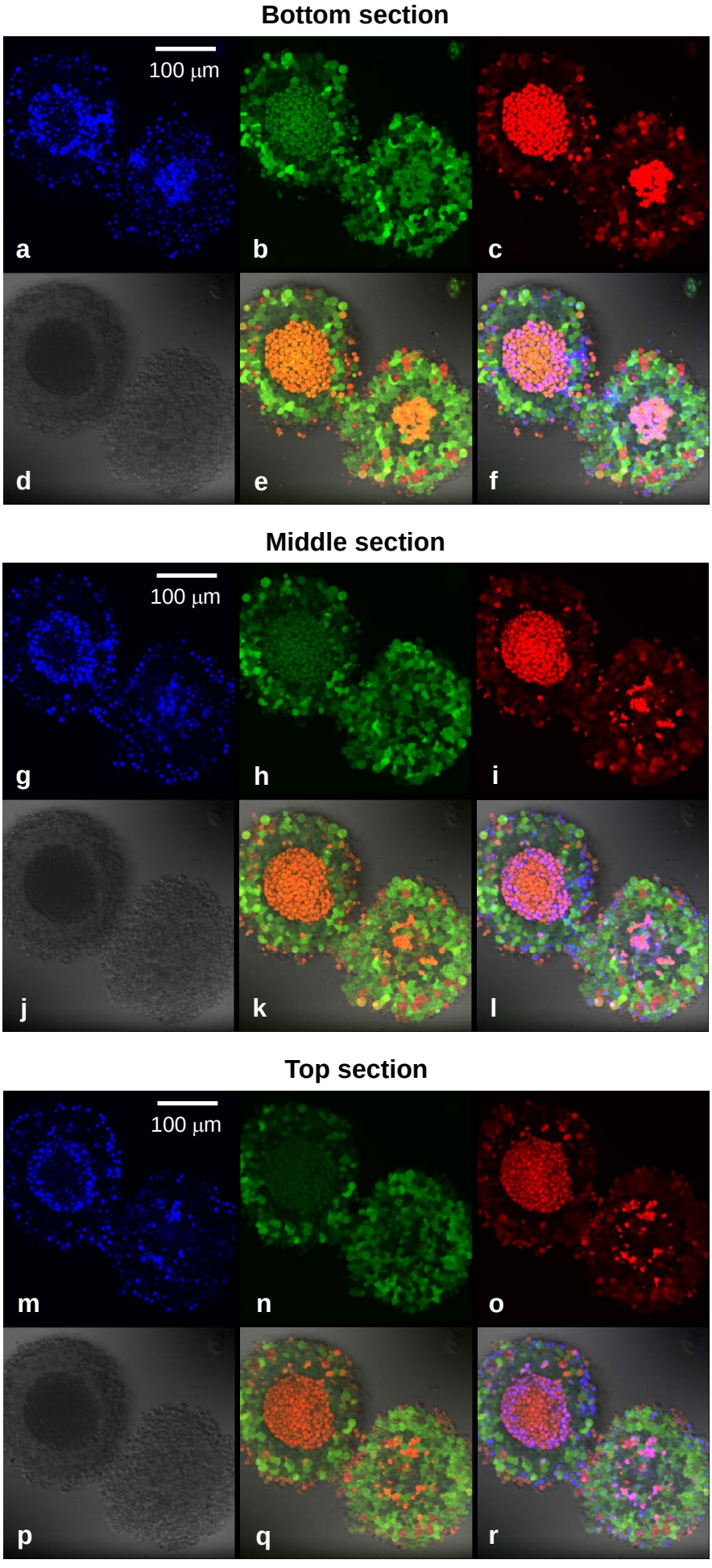

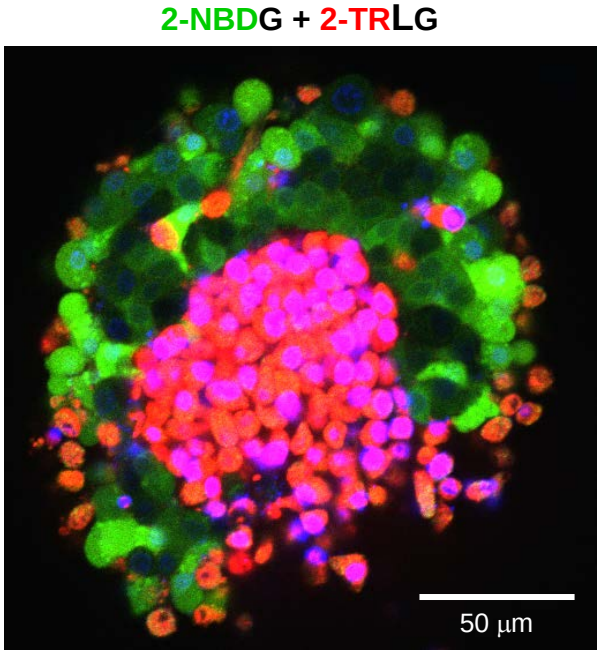

Online Resource 6. Confocal microscopic image of 13 DIV MIN6 spheroid taken at 4 minutes after starting washout of 100 μM of 2-NBDG (green) and 20 μM of 2-TRLG (red) mixture. Nuclei were stained by DAPI (blue). Note that dark and quiescent cells are somewhat less prominent in the surrounding area of the central core compared to those in Fig. 4l.

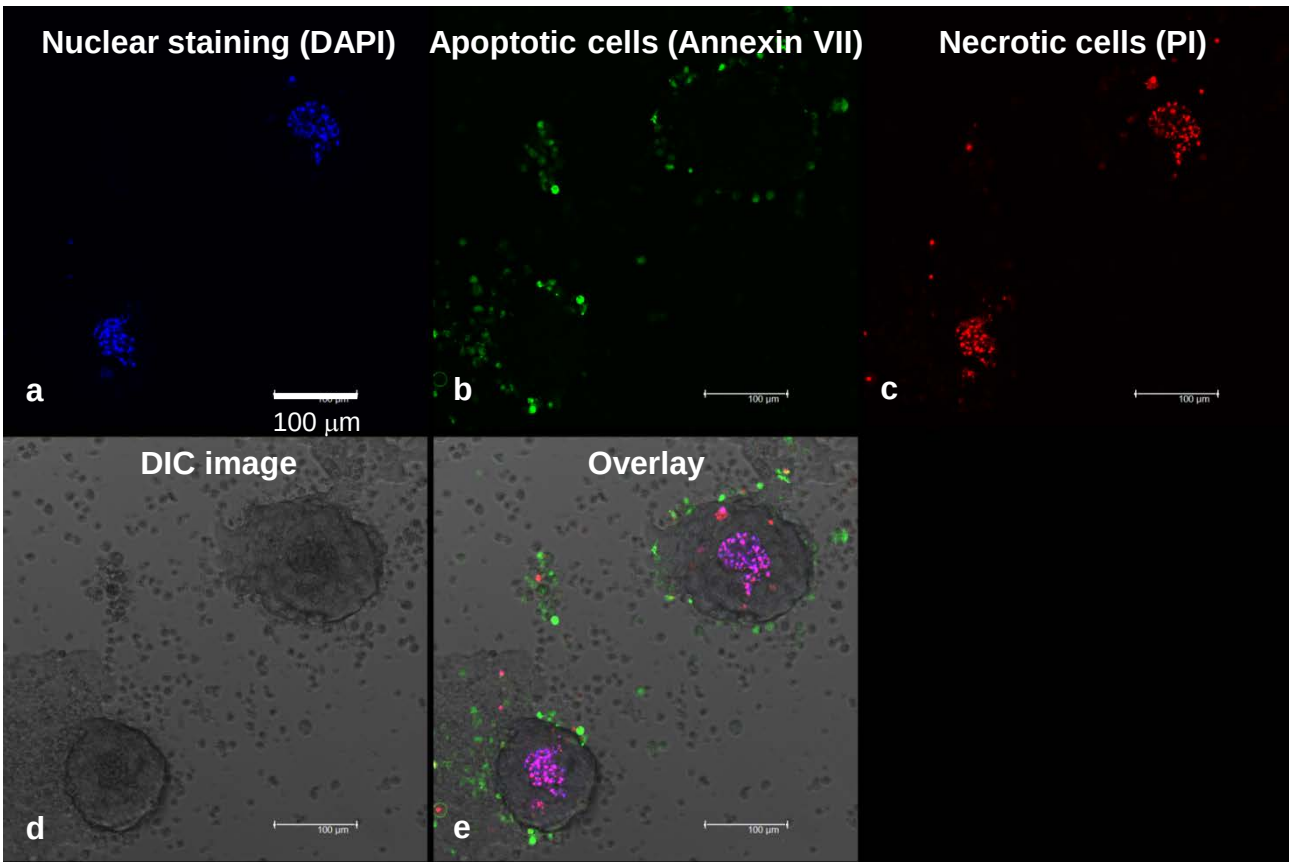

Online Resource 7. Representative MIN6 spheroids at 15 DIV including apoptotic and necrotic cells, each visualized by pSIVA-IANBD (green) and propidium iodide (PI, red), respectively, combined with DAPI staining during live imaging. **a**, Strongly DAPI-positive nuclei (blue) were seen mostly in the central core region of spheroids. **b**, Most pSIVA-IANBD-positive (green) apoptotic cells were seen in the outside of the spheroids. **c**, Most PI-positive (red) necrotic cells were localized in the central core of the spheroids. **d**, DIC image. **e**, Overlay. Scales are common to all panels.